analytical chemistry

pubs.acs.org/ac Article

# Alleviating Cell Lysate-Induced Inhibition to Enable RT-PCR from Single Cells in Picoliter-Volume Double Emulsion Droplets

Margarita Khariton,[▽] Conor J. McClune,[▽] Kara K. Brower, Sandy Klemm, Elizabeth S. Sattely, Polly M. Fordyce,* and Bo Wang*

Cite This: *Anal. Chem.* 2023, 95, 935−945 Read Online

ACCESS | Metrics & More | Article Recommendations | Supporting Information

**ABSTRACT:** Microfluidic droplet assays enable single-cell polymerase chain reaction (PCR) and sequencing analyses at unprecedented scales, with most methods encapsulating cells within nanoliter-sized single emulsion droplets (water-in-oil). Encapsulating cells within picoliter double emulsion (DE) (water-in-oil-in-water) allows sorting droplets with commercially available fluorescence-activated cell sorter (FACS) machines, making it possible to isolate single cells based on phenotypes of interest for downstream analyses. However, sorting DE droplets with standard cytometers requires small droplets that can pass FACS nozzles. This poses challenges for molecular biology, as prior reports suggest that reverse transcription (RT) and PCR amplification cannot proceed efficiently at volumes below 1 nL due to cell lysate-induced inhibition. To overcome this limitation, we used a plate-based RT-PCR assay designed to mimic reactions in picoliter droplets to systematically quantify and ameliorate the inhibition. We find that RT-PCR is blocked by lysate-induced cleavage of nucleic acid probes and primers, which can be efficiently alleviated through heat lysis. We further show that the magnitude of inhibition depends on the cell type, but that RT-PCR can proceed in low-picoscale reaction volumes for most mouse and human cell lines tested. Finally, we demonstrate one-step RT-PCR from single cells in 20 pL DE droplets with fluorescence quantifiable via FACS. These results open up new avenues for improving picoscale droplet RT-PCR reactions and expanding microfluidic droplet-based single-cell analysis technologies.

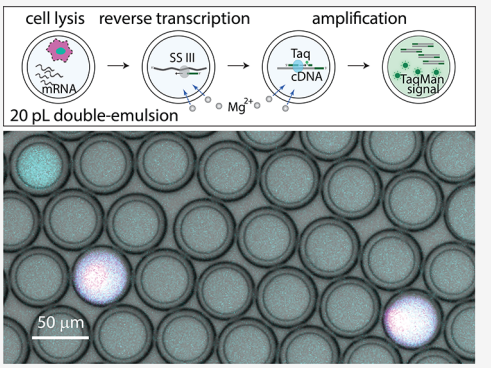


Downloaded via STANFORD UNIV on June 4, 2023 at 00:45:03 (UTC).
See https://pubs.acs.org/sharingguidelines for options on how to legitimately share published articles.

Encapsulation of cells within microfluidic droplets enables high-throughput genomic and transcriptomic profiling of individual cells through polymerase chain reaction (PCR) or sequencing-based techniques and has transformed many areas of biomedical research.[1−3] Cells are typically encapsulated within large water-in-oil single emulsion droplets (0.5−5 nL) as cell lysis within smaller volumes is commonly thought to inhibit downstream molecular biology reactions.[4−10] However, the ability to interrogate cells encapsulated within even smaller, picoliter droplets would confer several key advantages. First, it would significantly reduce the probability of encapsulating multiple cells in the same droplet.[11,12] Second, reducing the droplet size would proportionally lower the reagent costs. Finally, picoliter-volume compatibility would enable encapsulation of cells within aqueous-suspended double emulsions (water-in-oil-in-water) that can be sorted using commercially available fluorescence-activated cell sorter (FACS) instruments.[12−18] This development would allow biology laboratories without microfluidic expertise to perform droplet-based screens.

Small droplet size, however, poses a fundamental challenge. As the size of the droplet approaches that of a large cell (<1 nL), it has been reported that the increased concentration of cell lysate inhibits the molecular biology reactions essential for downstream analyses, including reverse transcription (RT) and PCR amplification.[4,19,20] Published reports of successful RT-PCR from single cells in droplets either used large volume (1 nL) droplets or diluted lysates before RT via droplet splitting and merging or picoinjection (Table S1).[6−10,21] However, the volume at which inhibition begins to emerge has not been rigorously quantified. It remains also ambiguous which steps of the RT-PCR reaction are inhibited and the degree to which and mechanism by which they are inhibited. A quantitative and systematic characterization of these inhibitory effects is required to mitigate them and guide the development of new droplet-based assays.

Here, we used Dropception[12] double emulsion (DE) droplets as picoliter-volume reactors for RT-PCR from single cells with the ability to screen DE droplets using FACS. To be compatible with standard FACS instruments, droplets must pass without clogging or shearing through FACS nozzles, constraining their maximum internal volume to ∼100 pL (∼60 μm diameter).[12,13,22] We systematically investigated every step of RT-PCR

**Received:** August 9, 2022
**Accepted:** December 13, 2022
**Published:** January 4, 2023


© 2023 American Chemical Society

https://doi.org/10.1021/acs.analchem.2c03475
*Anal. Chem.* 2023, 95, 935−945

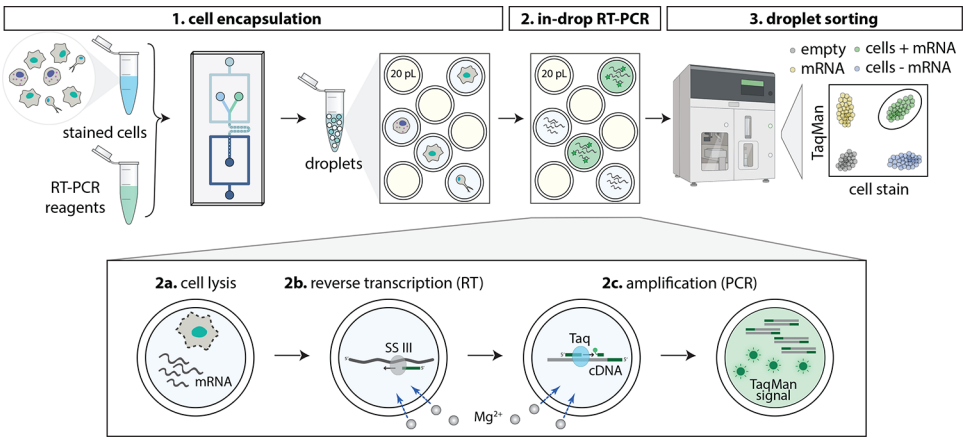


**Figure 1.** Workflow for single-cell RT-PCR in picoliter DE droplets. (1) Calcein AM-stained cells are coloaded into a microfluidic device with a TaqMan RT-PCR reagent mixture to form DEs of 20 pL internal volume surrounded by an aqueous carrier solution; (2) DEs are collected, pooled, and heated to drive RT for the targeted gene followed by PCR; and (3) DEs can be analyzed and sorted via standard flow cytometry to identify Calcein AM-positive, TaqMan-positive droplets containing cells expressing a transcript of interest.

reactions from single cells within small droplets and made several surprising findings.

First, we found that high concentrations of cell lysate in picoscale droplets led to cleavage of DNA probes, producing a false-positive signal and interfering with true amplification, which we mitigated by lysing cells via heat. Second, we found that RT-PCR was successful in the presence of surprisingly high lysate concentrations, though the efficiency dropped for low picoliter-volume reactions. Third, by quantifying amplification of exogenously supplemented RNA and DNA templates in the presence of lysates from a variety of human and mouse cell lines, we found that lysate-induced inhibition varied from no inhibition of RT to strong inhibition of PCR between cell lines. These insights and advances allowed us to demonstrate one-step RT-PCR directly from single cells in picoliter droplets, paving the way for new single-cell analysis technologies to isolate and enrich target cell populations based on gene expression signatures for downstream analyses.

## EXPERIMENTAL SECTION

Experimental details for standardized procedures, including cell culture, device fabrication and preparation, and image acquisition and analysis, are included in the Supporting Information.

**Double Emulsion Generation.** DE droplets were generated using four syringe pumps (PicoPump Elite, Harvard Apparatus) for cell suspension and inner, oil, and outer sheath solutions. The oil phase was composed of HFE7500 fluorinated oil (Sigma) and 2.2% Ionic PEG-Krytox (FSH, Miller–Stephenson).[23] The carrier phase contained 1% Tween-20 (Sigma) and 2% Pluronic F68 (Kolliphor 188, Sigma) in 1× phosphate-buffered saline (PBS). Prior to droplet loading, cells were stained with Calcein AM UltraBlue or DeepRed (AAT Bioquest), then resuspended to a concentration of $2.4 \times 10^6$/mL in 1× PBS supplemented with 20% OptiPrep (a density gradient medium to improve loading consistency) and 0.04% bovine serum albumin (BSA) for enzyme and droplet stabilization. Unless otherwise noted, the second inner phase contained 0.5× SuperScript III One-Step RT-PCR System buffer, 60 μL/mL SuperScript III RT/Platinum Taq High Fidelity mix (Thermo Fisher Scientific), 1% bovine serum albumin (BSA) (Fisher Scientific), 2 U/μL RNasin Ribonuclease Inhibitor (Promega), 1.2 μM PrimeTime primers, and 0.6 μM PrimeTime 5′ FAM/Zen/3′ IBFQ probe (IDT). Each phase was loaded into syringes (PlastiPak, BD) as described[12] and connected to the device via PE/2 tubing (Scientific Commodities). Typical flow rates were 400:100:105:6000 μL/h (oil/cells/reagents/outer).

**Droplet and Plate RT-PCR Assays.** Given the shell permeability of DE droplets,[18,23] we resuspended a 10 μL droplet pellet in 25 μL of 2× SuperScript III One-Step RT-PCR System buffer (unless otherwise noted) to transport key salt components in the buffer across the shell. RT-PCR reactions were performed as follows: 60 °C 90 min RT followed by 0 to 50 cycles of 94 °C 15 s, 50 °C 30 s, 68 °C 30 s. Droplet packing appeared to alter efficiency, with smaller numbers of droplets showing enhanced efficiency even when the ratio of droplet volume to total volume was kept constant (Figure S1); therefore, all droplet reactions were performed using total droplet pellet volumes of 10 μL.

Plate RT-PCR was performed using the same conditions on a CFX96 Real-Time PCR Detection System (BioRad) or an Applied Biosystems QuantStudio 3 (Thermo Fisher) with FAM fluorescence readout. Unless otherwise noted, the reagent mixture was composed of 1× SuperScript III One-Step RT-PCR System buffer, 30 μL/mL SuperScript III RT/Platinum Taq High Fidelity mix (Thermo Fisher Scientific), 0.5% BSA (Fisher Scientific), 1 U/μL RNasin Ribonuclease Inhibitor (Promega), 0.6 μM PrimeTime primers, 0.3 μM PrimeTime 5′ FAM/Zen/3′ IBFQ probe (IDT), and concentrated cell suspension for a final reaction volume of 10 μL. Primer sequences used are listed in Table S2. Concentrations of SuperScript and Taq enzymes were higher than those in standard RT-PCR, as higher concentrations improved the efficiency under conditions of high cell lysate concentrations. Cell suspensions were counted manually and then diluted to reach the desired concentration in 1× PBS supplemented with 0.04% BSA. mTurqouise DNA was synthesized as a gBlock (IDT) and amplified by PCR. mRNA was generated by in vitro T7 transcription (HiScribe T7, NEB). DNA and mRNA were added to the reaction mixture immediately before heat lysis.

To extract a scalar value ($C_i$, or cycle of inflection) from RT-qPCR and qPCR data, curves were fit to an asymmetric sigmoid[24] (scipy-optimize package)


https://doi.org/10.1021/acs.analchem.2c03475
Anal. Chem. 2023, 95, 935−945

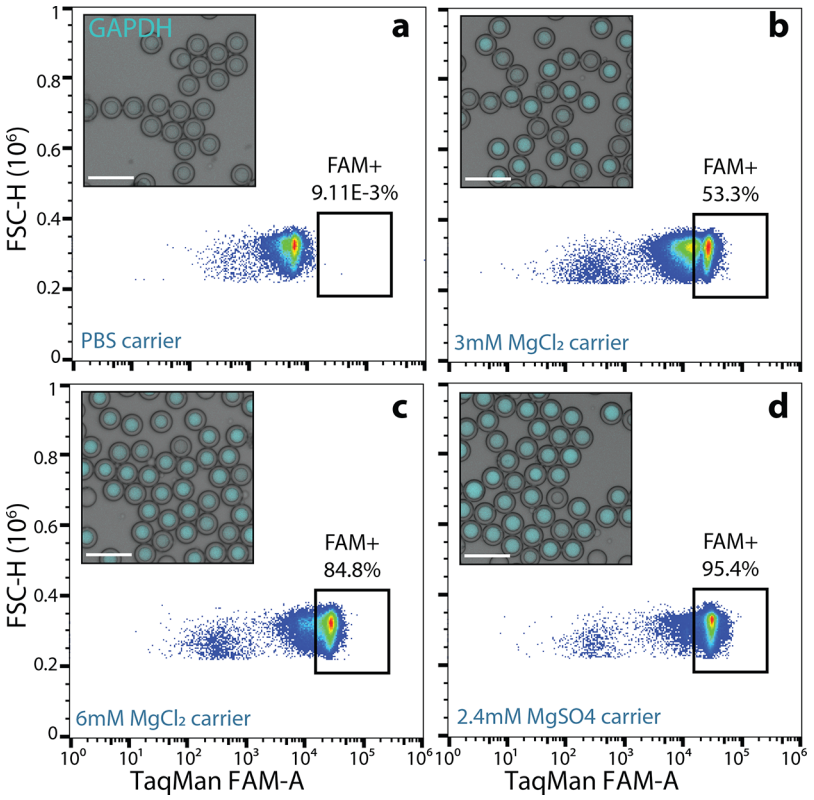


**Figure 2.** Efficiency of RT-PCR from purified RNA in DEs depends on the salt concentration of the carrier solution. FACS plots of DEs loaded with 1 pg/droplet K-562 cell total RNA and reagents for *GAPDH* RT-PCR after 50 PCR cycles when incubated in (a) 1× PBS with 2% Pluronic F68 and 1% Tween-20, (b) 1× M-MLV RT buffer (containing 3 mM $MgCl_2$), (c) 1× M-MLV RT buffer supplemented with an additional 3 mM $MgCl_2$, and (d) 2× Invitrogen One-Step RT-PCR buffer (containing 2.4 mM $MgSO_4$). The $FAM^+$ gate is shown with the fraction of $FAM^+$ droplets denoted; insets show representative merged bright-field and FAM fluorescence images of droplets for each sample. Scale bars: 100 $\mu$m.

$$g(x) = y_0 + \frac{(y_1 - y_0)}{(1 + \exp(b(x - C_i))^f}$$

The asymmetry parameter ($f$) was fixed at 0.3, which is the approximate value for most fits without fixing $f$, to improve the stability of curve fitting. Post-PCR electrophoresis was conducted on an Agilent Tapestation using High Sensitivity D1000 ScreenTape and 1:10 diluted PCR product.

**Double Emulsion Flow Cytometry.** DE droplets were analyzed via FACS as described in the prior sdDE-FACS[13] and Dropception[12] studies. One hundred microliters of droplets were resuspended in 500 $\mu$L of sheath buffer containing 1% Tween-20 (Sigma) in 1× PBS and analyzed on a SH800 flow cytometer (Sony) using a standard 408 nm laser configuration with a 130 $\mu$m nozzle. After a brief pickup delay time of ∼2 min, DEs were gated on FSC-H vs FSC-W and analyzed for Calcein AM and TaqMan FAM signal. All flow parameters are as previously reported.[12] FACS data were downsampled to 40,000 DEs and analysis performed with FlowJo software (v10).

## RESULTS AND DISCUSSION

**Dropception Single-Cell RT-PCR Workflow.** Our workflow (Figure 1): (1) coencapsulates cells and reagents including TaqMan probes within 20 pL DE droplets, (2) lyses cells, reverse transcribes mRNAs, and detects transcripts of interest via TaqMan PCR, and then (3) selects droplets containing cells expressing targeted transcripts via FACS. We chose a TaqMan assay instead of DNA intercalating dyes to prevent background signals from genomic DNA and cDNA. After isolation, droplets can be either air lysed into well plates or demulsified,[12,13] allowing cell selection based on transcript expression prior to downstream assays such as RNA sequencing.

To establish that this pipeline is compatible with standard RT-PCR as previously established,[25−30] we first tested the amplification of a housekeeping gene *GAPDH* from purified human RNA within droplets (1 pg/droplet). While DE droplets were stable after thermal cycling, reactions using buffers typical for RT-PCR within single emulsion droplets failed to generate fluorescence even after 50 cycles of amplification (Figure 2a). As RT and PCR enzymes are critically sensitive to the concentrations of ion cofactors (e.g., $MgCl_2$, $MgSO_4$, and Mn) and these ions can cross thin DE oil shells,[18,23,31] we supplemented the external PBS carrier solution with $MgCl_2$ or $MgSO_4$. This dramatically enhanced reaction efficiencies to ∼85% and >95%, respectively (Figures 2b−d and S1). As both Taq and SuperScript III can utilize $MgCl_2$ but $MgSO_4$ is a more efficient cofactor for Taq,[32] this enhancement likely results from increased Taq activity.

**Picoliter-Volume Droplet RT-PCR Reveals Lysate-Induced DNA Probe Cleavage.** Based on prior studies either reporting significant inhibition of RT-PCR within small (<1−5 nL) reaction volumes or diluting reaction volumes prior to RT,[4−10,19−21] we expected RT-PCR from single cells within 20 pL DEs to yield no signal. Unexpectedly, DEs loaded with human Jurkat T cells and TaqMan reagents to detect *GAPDH* displayed fluorescence in ∼80% of cell-containing droplets after only 20 cycles of PCR (Figure 3a). However, experiments using a probe specific to a sequence absent in the human genome also


https://doi.org/10.1021/acs.analchem.2c03475
Anal. Chem. 2023, 95, 935−945

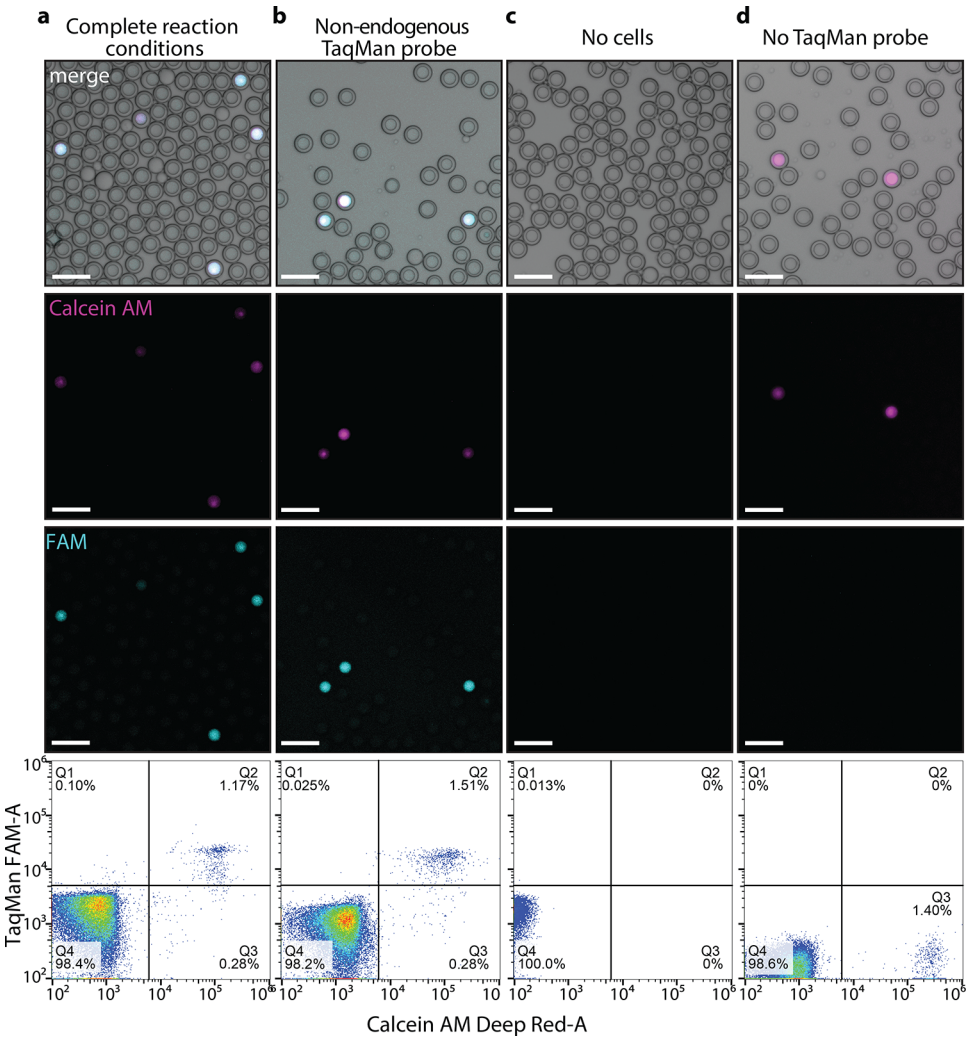


**Figure 3.** Lysate-induced probe cleavage within DE droplets. Representative bright field and fluorescence microscopy images (top: Calcein AM in magenta, TaqMan/FAM in cyan) and FACS analysis (bottom) for DE droplets loaded with (a) Calcein AM-stained Jurkat cells and complete reaction buffer (*GAPDH* TaqMan reagents and lytic detergents: 0.1% NP-40, 0.1% Tween-20, 0.01% Digitonin) after RT and 20 cycles of PCR, (b) Calcein AM-stained Jurkat cells and complete reaction buffer containing TaqMan probe and primers for a gene absent within human genome after RT and 20 cycles of PCR, (c) complete reaction buffer without cells, and (d) Calcein AM-stained Jurkat cells and reaction buffer without TaqMan probe and primers. FACS density plots display DE-gated droplets. DE gates for all FACS data are shown in Figure S2. Scale bars: 100 $\mu$m.

generated a strong fluorescence signal (Figure 3b), suggesting that the signal was not produced through PCR amplification of gene target. Consistent with this, cell-containing droplets exhibited similar fluorescence even without thermal cycling (Figure S3a) and in the absence of both Taq and SuperScript III enzymes (Figure S3b). This signal disappeared in the absence of cells (Figure 3c) or TaqMan probes (Figure 3d), indicating the fluorescence readout results from an interaction between cell lysate and TaqMan probes.

Unlike commonly expected mechanisms of PCR inhibition, which manifest as diminished or absent signal, this false-positive signal is consistent with nonspecific cleavage of the probe and release of the fluorophore from its quencher. Indeed, droplets suspended in $Mg^{2+}$-free buffers yielded weak signals (Figure S3c) consistent with probe cleavage via endogenous cellular enzymes (e.g., DNases).

**Heat Inactivation Alleviates Premature Probe Cleavage.** To enable more rapid and systematic testing of picoliter-volume conditions, we next tested whether the lysate-induced probe cleavage observed in droplets could be replicated within multiwell plates containing high cell lysate concentrations[8] (Figure 4a). To mimic the volume ratio within DEs, we generated 10 $\mu$L reactions containing 500,000 cells, yielding an effective lysate concentration equivalent to a single cell in a 20 pL droplet. The inclusion of even gentle nonionic lysis detergents such as NP-40[33] led to instantaneous probe cleavage in the absence of amplification, observable as a high baseline fluorescence prior to thermal cycling, consistent with lysate-mediated digestion of DNA probes (Figure 4b). In contrast, cells incubated with RT-PCR reagents in the absence of NP-40 showed no probe cleavage until the start of the amplification, suggesting that alternative lysis methods could eliminate premature probe cleavage.

Prior reports suggested that heat treatment alone can lyse cells.[33] We therefore attempted to identify conditions capable of driving efficient lysis and simultaneously inactivating endogenous DNases without denaturing the enzymes required for RT and PCR (Figure 4c). While incubation at either 4 or 20 °C for 30 min had no effect on premature probe cleavage (visible as high fluorescence prior to amplification), incubation at 60 °C or


https://doi.org/10.1021/acs.analchem.2c03475
Anal. Chem. 2023, 95, 935−945

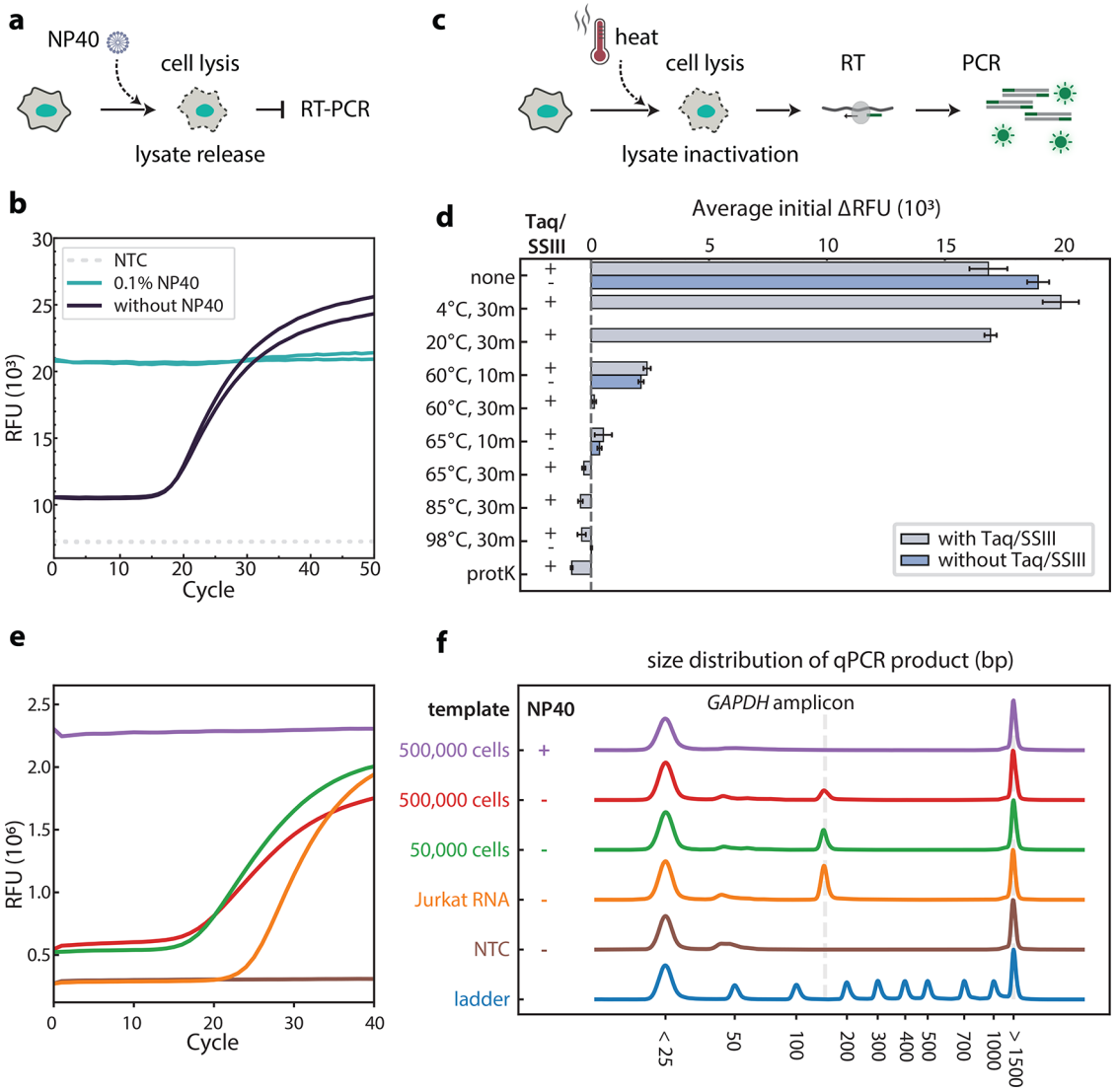


**Figure 4.** Heat inactivation mitigates lysate-induced probe cleavage. (a) Schematic illustrating cell lysis and subsequent lysate release upon addition of NP-40, inhibiting RT-PCR. (b) Traces of plate-based TaqMan *GAPDH* RT-qPCR reactions at high lysate concentrations (500,000 Jurkat cells per 10 $\mu$L). Reactions containing 0.1% NP-40 exhibit the high initial relative fluorescence unit (RFU) prior to PCR, indicating premature probe cleavage, and no amplification. NTC: no template control. (c) Schematic illustrating an initial heat treatment of cells prior to RT-PCR to simultaneously lyse cells and inactivate cleavage-inducing factors in cell lysate. (d) Average initial RFU values above the baseline of the first 3 PCR cycles (normalized to no probe control) with detergent-free conditions for 500,000 cells per 10 $\mu$L; probe cleavage is visible as a high initial RFU value. Cells were incubated at the indicated temperatures and times or with 0.5 mg/mL proteinase K (proK, 65 °C, 15 min incubation followed by 85 °C, 15 min inactivation) prior to combining with the reaction mixture. Color of bars: whether the reactions took place in the presence or absence of enzymes; error bars: standard deviation. (e) Traces of TaqMan *GAPDH* RT-qPCR using Jurkat cells or pure RNA after heat lysis at 60 °C for 90 min, with or without NP-40. (f) Electrophoresis showing the size distribution of products from RT-qPCR reactions in panel (e), with colors labeling matched samples. The dominant product matches the expected 143 bp *GAPDH* amplicon and is absent with NP-40.

higher for 30 min or longer largely eliminated it (Figure 4d), consistent with the fact that non-thermophilic endogenous proteins typically denature between 40 and 70 °C.[34] We therefore chose to heat-inactivate at 60 °C for 90 min to ensure maximal cell lysis for all subsequent assays; importantly, this condition is also optimal for reverse transcriptase activity, permitting a single step for lysis and cDNA production. We still observed a slightly decreased dynamic range for the fluorescence signal likely due to small amounts of lysate-induced probe cleavage prior to heat inactivation. Consistent with the TaqMan signal (Figure 4e), electrophoresis showed robust amplification of the correct PCR product only in the absence of NP-40 (Figure 4f). The reaction proceeded even at high cell concentrations (i.e., 500,000 cells per 10 $\mu$L, equivalent to 1 cell per 20 pL droplet).

**Distinct Cell-Type-Dependent Regimes of Single-Cell RT-PCR.** The plate-based assay also allowed us to vary cell lysate concentration and quantify the RT-PCR efficiency (Figure 5a). To quantify amplification from qPCR curves with differing baseline and saturation, we fit curves to an asymmetric sigmoid and used the cycle of inflection point ($C_i$), instead of $C_t$, cycle threshold, which was difficult to consistently quantify across curves with different shapes and amplitudes.[24] With Jurkat cells, $C_i$ scaled with cell number over several distinct regimes (Figure 5b). Reactions with 30,000 cells or fewer in 10 $\mu$L (equivalent of single cells in droplets > 300 pL) followed the expected log-


https://doi.org/10.1021/acs.analchem.2c03475
Anal. Chem. 2023, 95, 935−945

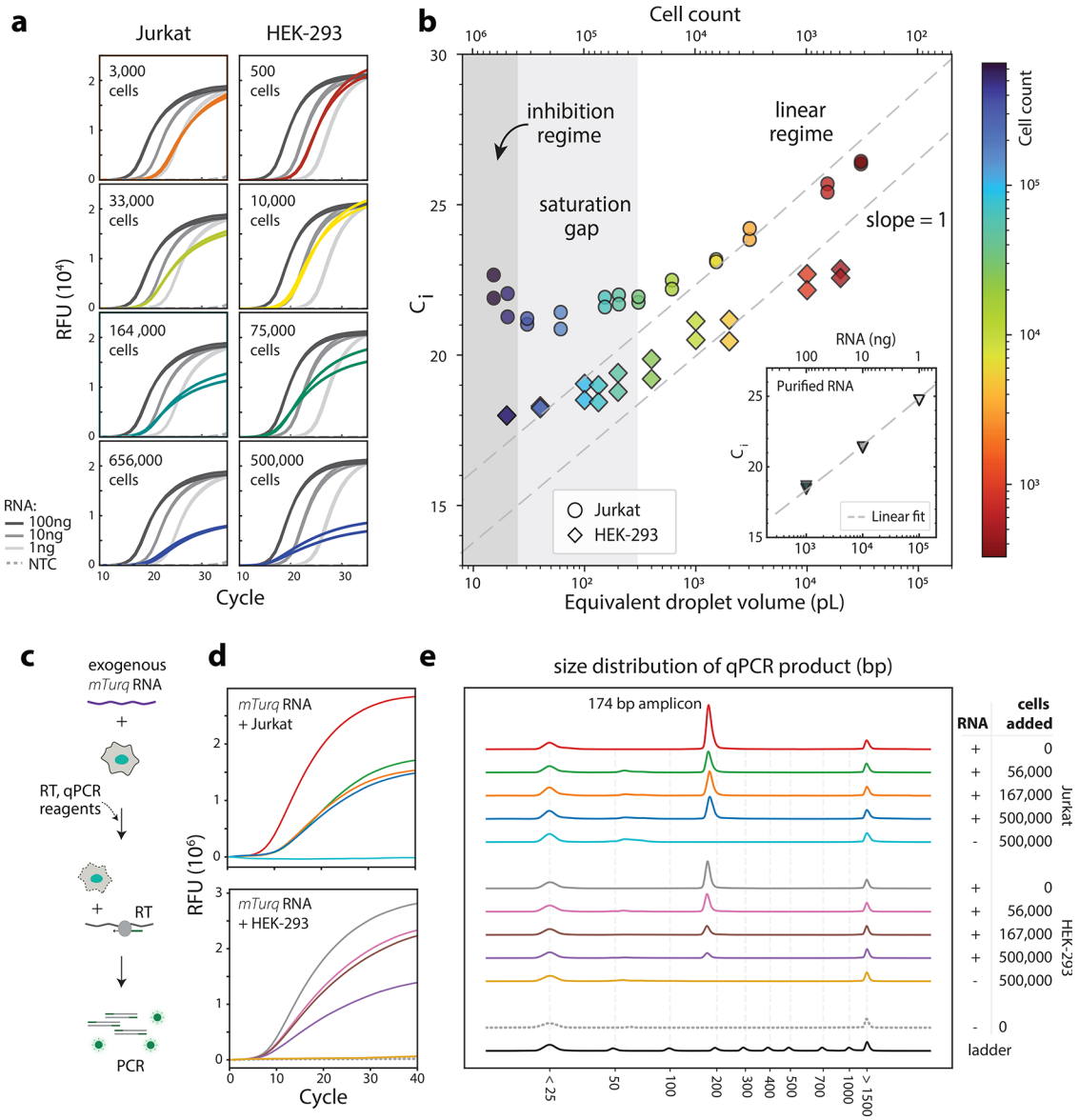


**Figure 5.** RT-PCR reaction efficiency depends on cell lysate concentration. (a) Baseline-subtracted qPCR traces for 10 $\mu$L reactions containing 500–656,000 cells (equivalent to 1 cell in a 400 nL to 15 pL droplet, respectively) detecting *GAPDH* transcripts (colored traces). Cell were lysed via heat. Gray lines: amplification of purified Jurkat RNA; dashed lines: no template control (NTC). (b) $C_i$ values for a range of Jurkat or HEK-293 cell counts in a 10 $\mu$L reaction plotted as a function of the equivalent single-cell-loaded droplet volume. Inset: purified Jurkat RNA controls. Dashed lines: theoretical log-linear relationship between $C_i$ and cell count with a slope of 1. (c) Schematic for RNA spike-in experiment. (d) Traces of RT-qPCR from 100 pM *mTurquoise* RNA mixed with different numbers of Jurkat or HEK-293 cells in 10 $\mu$L reactions. (e) Electrophoresis showing the size distribution of products from RT-qPCR reactions in panel (d), with colors labeling matched samples.

linear trend in $C_i$ as observed for purified RNA. Below the equivalent droplet size of 300 pL, $C_i$ values began to plateau. At even higher concentrations (>328,000 cells in 10 $\mu$L, equivalent to 1 cell in a <30 pL droplet), $C_i$ increased with increasing cell numbers, suggesting that within this "inhibition" regime, lysate-induced inhibition began to block the reaction. However, even at very high lysate concentrations, amplification traces indicate successful reactions, contrary to prior claims of pervasive inhibition in small volumes.[4,19,20]

By contrast, human embryonic kidney (HEK-293) cells only showed a minor deviation off the log-linear trend when the cell number exceeded 100,000 (equivalent to single cells in 100 pL droplets), indicating moderate RT-PCR inhibition (Figure 5a,b). Even higher effective lysate concentrations did not yield an inhibition regime in which $C_i$ values increases with increasing cell concentrations.

To verify amplification of the desired PCR product, we added 100 pM of exogenous RNA template (*mTurquoise*) into 10 $\mu$L RT-PCR reactions with varying numbers of cells (Figure 5c). The TaqMan signal (Figure 5d) correlated with the abundance of the expected product measured via DNA fragment analysis, even though the PCR product concentration decreased with the number of cells added (Figure 5e). These results establish unambiguously that lysate-induced inhibition in picoscale volumes is neither significant nor ubiquitous but rather depends on cell type.

**Quantifying the Degree of Inhibition of RT-PCR in Various Cell Lines.** Understanding the source of inhibition is critical for identifying strategies to alleviate it and for assessing


https://doi.org/10.1021/acs.analchem.2c03475
Anal. Chem. 2023, 95, 935−945

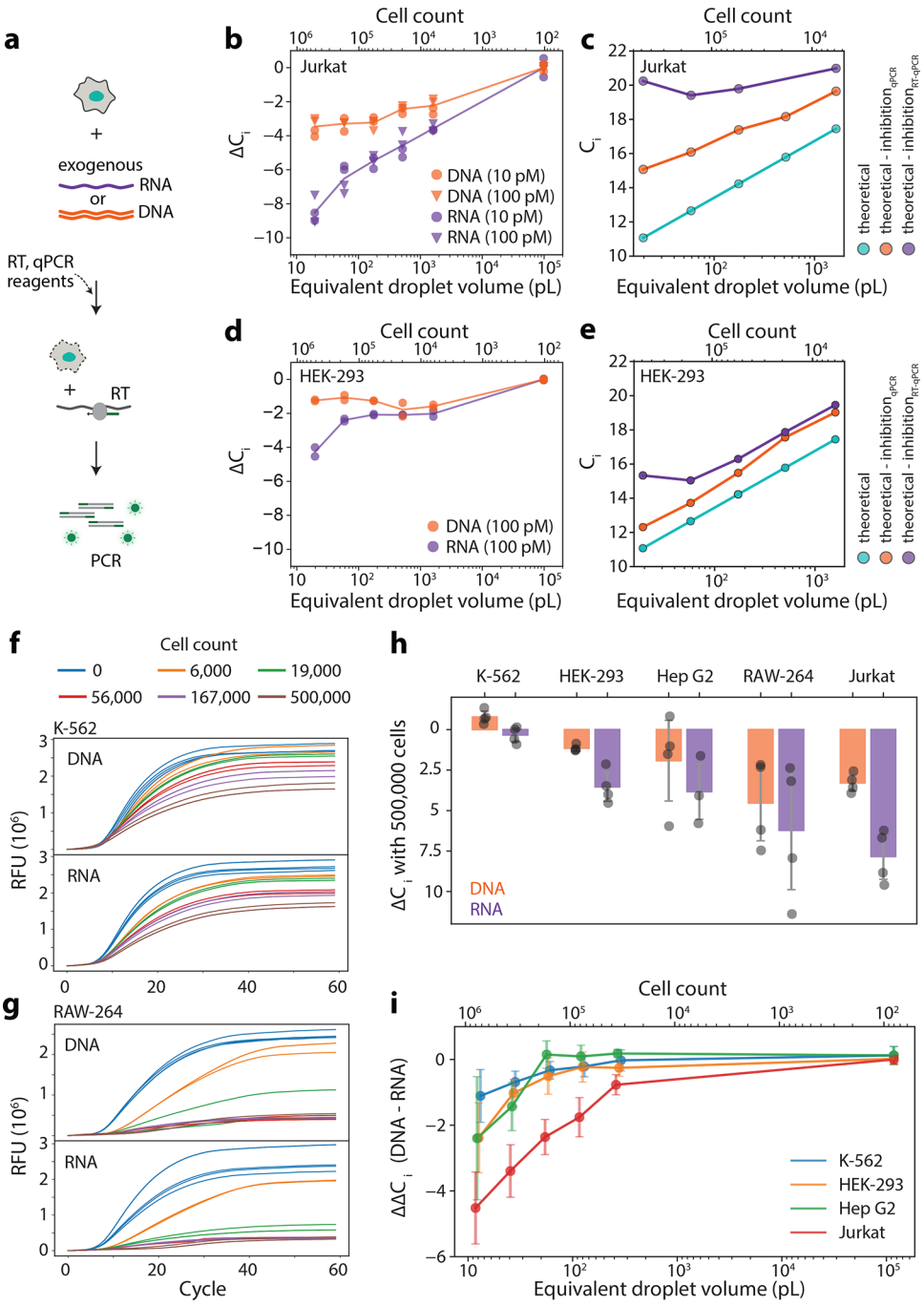


**Figure 6.** Quantifying the degree to which RT-PCR is inhibited at RT and PCR steps. (a) Schematic of the assay quantifying lysate-induced inhibition of PCR or RT-PCR using exogenous supplemented DNA and mRNA, respectively. (b) Inhibition of PCR (orange) or RT-PCR (purple), quantified as changes in $C_i$ ($\Delta C_i$) for exogenous DNA and mRNA templates in the presence of Jurkat cells. (c) Theoretically expected $C_i$ for endogenous transcripts whose abundance should scale linearly with cell number (cyan); subtracting expected inhibitory effects on PCR (orange) and on RT-PCR (purple) measured in panel (b), which reproduces observed amplification regimes (inhibition, saturation, and linear regimes) for Jurkat cells shown in Figure 5b. (d) Measured inhibition of PCR and RT-PCR vs HEK-293 cell concentration. (e) Expected $C_i$ of endogenous transcripts for HEK-293 cells, showing no inhibition regime. (f, g) Baseline-subtracted qPCR traces with exogenous DNA or mRNA templates with increasing concentrations of (f) K-562 and (g) RAW264 cells. (h) $\Delta C_i$ between 0 and 500,000 cells for five cell lines quantified using either exogenous DNA (PCR) or mRNA (RT-PCR) templates. (i) $\Delta\Delta C_i$, the difference between inhibition measured using DNA vs mRNA templates, quantifies inhibition of RT as a function of cell concentrations for four cell lines. RAW264 cells are excluded due to complete inhibition of PCR at high lysate concentrations.

feasibility of downstream applications. For example, efficient cell lysis and RT is already sufficient for constructing RNAseq libraries in low-volume droplets, while sorting and sequencing only droplets containing cells expressing a target transcript requires efficient RT and in-drop PCR. We therefore attempted to quantify the relative contributions of each step of RT-PCR to its reduced overall efficiency.

Since heat is reported to be an inefficient means of cell lysis,[33] we first tested if RT efficiency is limited by incomplete lysis. The addition of 0.1% NP-40 after heat lysis did not enhance RT-PCR signal (Figure S4a,b) even though this concentration of NP-40 is


https://doi.org/10.1021/acs.analchem.2c03475
Anal. Chem. 2023, 95, 935−945

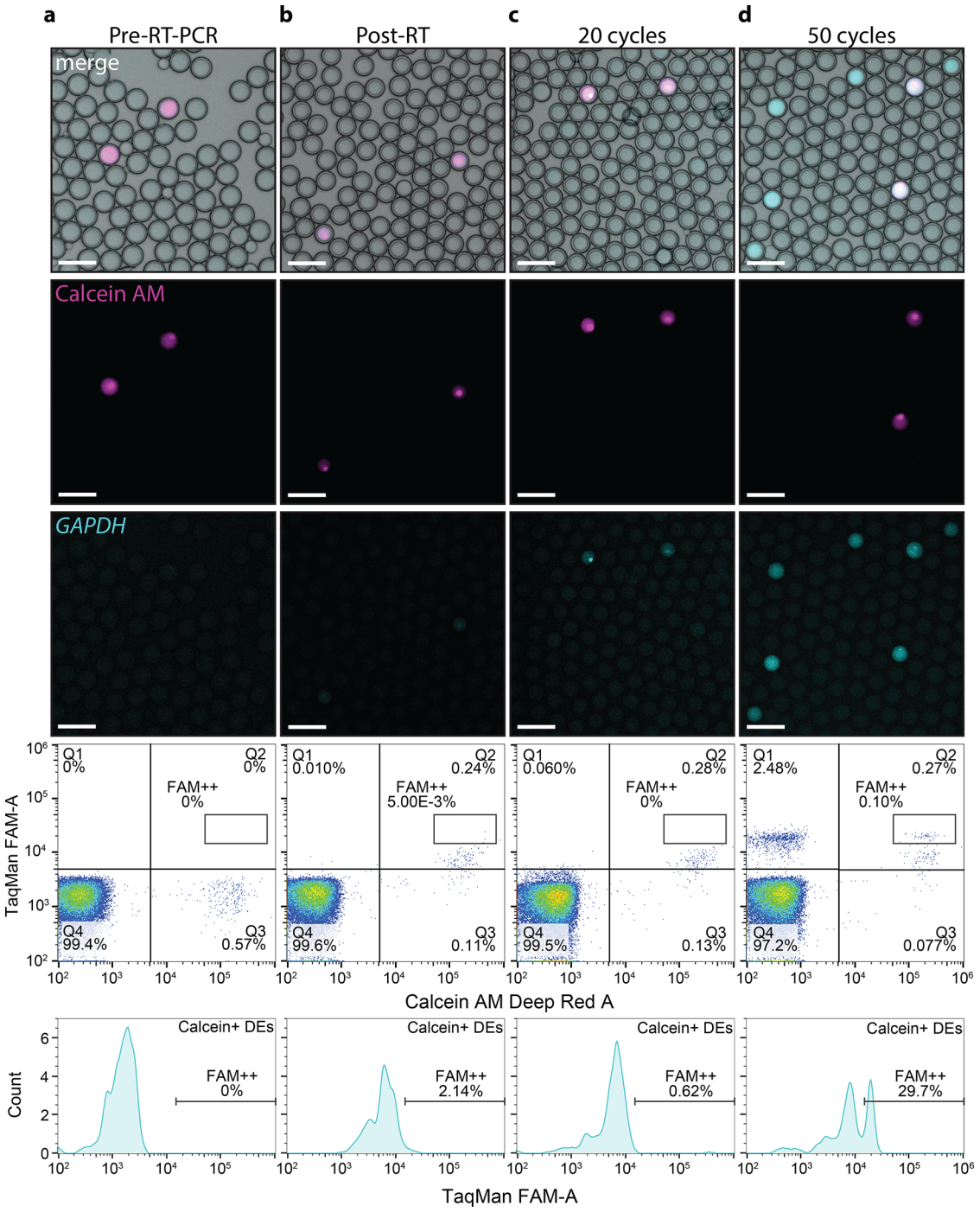


**Figure 7.** One-step RT-PCR from single cells encapsulated within 20 pL DE droplets. Representative bright-field and fluorescence microscopy images (top: Calcein AM in magenta, TaqMan/FAM in cyan) and FACS plots (bottom) for DEs loaded with Calcein AM-stained Jurkat cells and TaqMan RT-PCR reagents for *GAPDH* using the optimized RT-PCR condition. Histograms show distributions of FAM fluorescence in Calcein$^{+}$ DEs, with the fraction of high FAM$^{++}$ population denoted. Columns correspond to (a) prior to RT-PCR, (b) after heat lysis and RT but prior to PCR, (c) after 20 PCR cycles, and (d) after 50 PCR cycles. Scale bars: 100 $\mu$m.

documented to be highly effective to lyse cells.[8,26,33] Furthermore, mechanical shearing of cells by pipetting did not improve amplification (Figure S4c,d). These data suggest that cell lysis was not limiting in our assay. To ensure that the amplification efficiency loss was not due to RNA hydrolysis during heat treatment, we amplified purified RNA via RT-PCR with and without the 60 °C treatment step and confirmed that efficiency was unchanged (Figure S4e,f). Finally, increasing concentrations of TaqMan probe (Figure S4g) or primers (Figure S4h) did not enhance the PCR efficiency, although increased probe concentration resulted in significantly higher background (Figure S4g), suggesting that primer/probe sequestration or cleavage is no longer a source of inhibition after heat inactivation.

Next, we examined the efficiency of the RT and PCR steps separately. To determine the degree to which PCR alone is inhibited by cell lysate, we spiked in known amounts of an exogenous DNA (*mTurquoise*) into 10 $\mu$L reactions containing


https://doi.org/10.1021/acs.analchem.2c03475
Anal. Chem. 2023, 95, 935−945

up to 500,000 cells (Figure 6a) and quantified amplification using $C_i$ (Figure S5). Independent of the template concentration, qPCR amplification lagged by ∼2 cycles with 6,000 cells in 10 μL (equivalent to single cells in 2 nL droplets) and ∼4 cycles with 500,000 cells (equivalent to single cells in 20 pL droplets) (Figure 6b). Spiking in known amounts of *mTurquoise* mRNA revealed comparable inhibition at the RT step: amplification was further delayed by ∼2 cycles with 6,000 added cells and ∼5 cycles with 500,000 cells (Figure 6b). This RT and PCR inhibition explains the linear, saturation, and inhibition regimes observed when amplifying endogenous transcripts from Jurkat cells. Without inhibition, $C_i$ for RT-PCR of an endogenous transcript should increase log-linearly with the number of cells. Subtracting the measured loss from the expected $C_i$ (Figure 6c) reproduced the observed relationship between cell concentration and amplification with *GAPDH* probes (Figure 5b).

HEK-293 cell lysate was much less inhibitory, even though it has a ∼50% larger volume compared to Jurkat cells, leading to higher lysate concentrations with the same number of cells added. When adding 500,000 HEK-293 cells to a 10 μL reaction, RT and PCR was inhibited by only ∼2 cycles at each step (Figure 6d), comparable to the degree of inhibition with 6,000 Jurkat cells. These mild losses were in quantitative agreement with the complete absence of an inhibitory regime observed with *GAPDH* probes (Figures 6e and 5b), suggesting that HEK-293 cell lysate is ∼100-fold less inhibitory and may be more amenable to RT-PCR in smaller droplets than Jurkat cells.

The large and unexpected difference between two cell types motivated us to survey additional cell lines including bone marrow lymphoblasts (K-562), hepatocellular carcinoma cells (Hep G2), and murine macrophages (RAW264) (Figure S5). K-562 cells displayed only minimal PCR inhibition (Figure 6f); RAW264 cells were most inhibitory to PCR, with >50,000 cells per 10 μL reaction essentially precluding amplification (Figure 6g). Except RAW264, all other cell lines tested showed significantly lower inhibition than Jurkat cells. When 500,000 cells were added, the reaction with K-562 cells displayed <1 cycle loss for both PCR and RT-PCR, suggesting almost no inhibition of RT; addition of 500,000 Hep G2 cells inhibited PCR by ∼2 cycles and RT by ∼2 additional cycles, similar to HEK-293 cells (Figure 6h). This variability was consistent across lysate concentrations and inhibition to RT was mostly minimum except at high lysate concentrations (Figure 6i).

Surprisingly, common strategies to improve stability and activity of reverse transcriptase and Taq polymerase (i.e., adding additional $Mg^{2+}$, EGTA, and dithiothreitol), had little or even inhibitory effects (Figure S6a−c). While prior work reported that adding single-stranded DNA-binding proteins (SSBs) can mitigate RT-PCR inhibition in 1 nL volumes,[8] we found no improvement under conditions mimicking picoliter volumes (Figure S6d). Adding extra RT or PCR enzymes decreased $C_i$ by 1−2 cycles (Figure S6e,f), suggesting that RT-PCR reaction efficiency can be further improved. Together, our results demonstrate that cell lysate-mediated inhibition of PCR and RT is cell-type-dependent, yet generally low enough to allow single-cell RT-PCR in picoliter droplets.

**Picoliter-Volume Droplet One-Step RT-PCR from Single Cells.** To test whether single-cell RT-PCR can proceed in picoliter DEs under optimized conditions, we coloaded Jurkat cells, one of the most inhibitory cell lines, with TaqMan RT-PCR reagents and probes for *GAPDH* transcripts and quantified TaqMan fluorescence before RT, after RT, and after either 20 or 50 PCR cycles (Figure 7). The amplicon spanned a 1632 bp intron to ensure that the fluorescence signal resulted from amplification of cDNA and not genomic DNA. Droplets exhibited no background TaqMan fluorescence prior to thermal cycling, remaining stable even after several hours in solution (Figure 7a). Upon heat lysis, cell-containing droplets began to show low background fluorescence (Figure 7b), consistent with the remnant lysate-induced probe cleavage. Following 20 cycles of PCR, microscopy images of droplets showed increased FAM intensities, but this signal remained indistinguishable from background fluorescence in FACS analysis (Figure 7c) and significantly lower than the false-positive signals observed without heat inactivation (Figure 3a,b).

After 50 cycles of PCR, ∼30% of cell-containing droplets exhibited a distinct $FAM^{++}$ population, which was easily visible both via microscopy and FACS (Figure 7d). As 50 cycles of PCR is an over-amplification—performed to find the detection limit of true signal—we also observed FAM-positive, Calcein AM-negative droplets, signifying digital droplet PCR amplification of stray transcripts released from dead cells;[5] however, these were easily distinguishable from true positive droplets by Calcein signal and were present at a very low abundance (∼2.5% of the droplets that did not contain a cell) (Figure 7d). Omitting both Taq and SuperScript III enzymes eliminated the $FAM^{++}$ population, and the background fluorescence levels did not change between the heat lysis and amplification steps (Figure S7). Together, these data demonstrate successful RT-PCR from single cells in picoliter-volume reactions.

## CONCLUSIONS

The ability to sort cells based on their RNA content could allow selective recovery of cells of interest such as rare cell types revealed via single-cell transcriptomic studies,[35] cells containing latent integrated viruses,[36] and cells expressing RNA splice isoforms or noncoding RNAs.[37] While encapsulating single cells within DE droplets provides a promising method,[12−18] realizing this technology requires successful RT-PCR from single cells within small volumes (<100 pL). Here, we characterized and optimized RT-PCR reaction conditions and enable amplification from single cells encapsulated within FACS-sortable DE droplets. The developed protocol should be broadly applicable to other picoscale reactors.[38]

Ultimately, downstream recovery of transcriptomic information from isolated cells will require the ability to integrate single-cell RNAseq (scRNA-seq) library preparation into this pipeline. Although the temperature cycling required for TaqMan PCR may degrade labile RNA, inclusion of poly-dT primers during the initial RT step could convert all polyadenylated mRNA to more stable cDNA. After sorting DE droplets to multiwell plates, scRNA-seq library construction could proceed from recovered cDNA using standard techniques that employ well-based barcoding. Nevertheless, our results suggest that RT and PCR steps may be sufficiently efficient for the preparation of scRNA-seq libraries within sub-nanoliter double emulsion droplets, though additional studies will be required to determine detection sensitivity as a function of cell type, transcript abundance, and droplet size.

## ASSOCIATED CONTENT

### Supporting Information

The Supporting Information is available free of charge at https://pubs.acs.org/doi/10.1021/acs.analchem.2c03475.



https://doi.org/10.1021/acs.analchem.2c03475
Anal. Chem. 2023, 95, 935−945

DE droplet RT-PCR requires additional $Mg^{2+}$ in the carrier solution and needs to be performed in small volumes; DE gates used in FACS analysis; false positives of RT-PCR in DE droplets are still present without RT and PCR steps but absent when using carrier buffer without magnesium; reduced efficiency of RT-PCR is not due to insufficient lysis, RNA hydrolysis, or sequestration of primers/probes; lysate-induced inhibition of RT-PCR varies between cell lines; cell lysate-induced inhibition is not mitigated by additional $Mg^{2+}$, EGTA, DTT, or SSB protein, but RT-PCR can benefit from additional enzymes; optimized one-step droplet RT-PCR protocol eliminates lysate-induced probe cleavage and false positives; prior work claiming or consistent with lysate-mediated inhibition of reverse transcription from single cells in small volumes; and sequences of primers and probes (PDF)

## AUTHOR INFORMATION


### Corresponding Authors

**Polly M. Fordyce** − *Department of Bioengineering, Stanford University, Stanford, California 94305, United States; Department of Genetics and ChEM-H Institute, Stanford University, Stanford, California 94305, United States; Chan Zuckerberg Biohub, San Francisco, California 94110, United States;* orcid.org/0000-0002-9505-0638; Email: pfordyce@stanford.edu

**Bo Wang** − *Department of Bioengineering, Stanford University, Stanford, California 94305, United States;* orcid.org/0000-0001-8880-1432; Email: wangbo@stanford.edu

### Authors

**Margarita Khariton** − *Department of Bioengineering, Stanford University, Stanford, California 94305, United States*

**Conor J. McClune** − *Department of Chemical Engineering and Howard Hughes Medical Institute, Stanford University, Stanford, California 94305, United States*

**Kara K. Brower** − *Department of Bioengineering, Stanford University, Stanford, California 94305, United States*

**Sandy Klemm** − *Department of Genetics, Stanford University, Stanford, California 94305, United States*

**Elizabeth S. Sattely** − *Department of Chemical Engineering and Howard Hughes Medical Institute, Stanford University, Stanford, California 94305, United States;* orcid.org/0000-0002-7352-859X

Complete contact information is available at: https://pubs.acs.org/10.1021/acs.analchem.2c03475

### Author Contributions

[▽]M.K. and C.J.M contributed equally to this work.


### Notes

The authors declare no competing financial interest.

## ACKNOWLEDGMENTS

The authors thank R.N. Hall for technical assistance. This work is supported by a HFSP grant RGY0085/2019 (B.W.) and NIH grant 1DP2GM123641 (P.M.F.). M.K. is a BioX SIGF Lavidge and McKinley Fellow and a Siebel Scholar. C.M. is supported by the Damon Runyon Cancer Research Foundation (DRG-2421-21). P.M.F. is a Chan Zuckerberg Biohub Investigator. B.W. is a Beckman Young Investigator.

## REFERENCES


(1) Stuart, T.; Satija, R. *Nat. Rev. Genet.* **2019**, *20*, 257−272.
(2) Zhang, X.; Li, T.; Liu, F.; Chen, Y.; Yao, J.; Li, Z.; Huang, Y.; Wang, J. *Mol. Cell* **2019**, *73*, 130−142.e5.
(3) Svensson, V.; Vento-Tormo, R.; Teichmann, S. A. *Nat. Protoc.* **2018**, *13*, 599−604.
(4) White, A. K.; VanInsberghe, M.; Petriv, O. I.; Hamidi, M.; Sikorski, D.; Marra, M. A.; Piret, J.; Aparicio, S.; Hansen, C. L. *Proc. Natl. Acad. Sci. U.S.A.* **2011**, *108*, 13999−14004.
(5) Eastburn, D. J.; Sciambi, A.; Abate, A. R. *Nucleic Acids Res.* **2014**, *42*, No. e128.
(6) Eastburn, D. J.; Sciambi, A.; Abate, A. R. *Anal. Chem.* **2013**, *85*, 8016−8021.
(7) Kim, S. C.; Clark, I. C.; Shahi, P.; Abate, A. R. *Anal. Chem.* **2018**, *90*, 1273−1279.
(8) Ma, J.; Tran, G.; Wan, A. M. D.; Young, E. W. K.; Kumacheva, E.; Iscove, N. N.; Zandstra, P. W. *Sci. Rep.* **2021**, *11*, No. 6777.
(9) Chovancova, P.; Merk, V.; Marx, A.; Leist, M.; Kranaster, R. *Biol. Methods Protoc.* **2017**, *2*, No. bpx008.
(10) Zhu, Y.; Zhang, Y. X.; Liu, W. W.; Ma, Y.; Fang, Q.; Yao, B. *Sci. Rep.* **2015**, *5*, No. 9551.
(11) Collins, D. J.; Neild, A.; deMello, A.; Liu, A.-Q.; Ai, Y. *Lab Chip* **2015**, *15*, 3439−3459.
(12) Brower, K. K.; Khariton, M.; Suzuki, P. H.; Still, I. I. C.; Kim, G.; Calhoun, S. G. K.; Qi, L. S.; Wang, B.; Fordyce, P. M. *Anal. Chem.* **2020**, *92*, 13262−13270.
(13) Brower, K. K.; Carswell-Crumpton, C.; Klemm, S.; Cruz, B.; Kim, G.; Calhoun, S. G. K.; Nichols, L.; Fordyce, P. M. *Lab Chip* **2020**, *20*, 2062−2074.
(14) Aharoni, A.; Amitai, G.; Bernath, K.; Magdassi, S.; Tawfik, D. S. *Chem. Biol.* **2005**, *12*, 1281−1289.
(15) Chong, D.; Liu, X.; Ma, H.; Huang, G. Y.; Han, Y. L.; Cui, X. Y.; Yan, J. J.; Xu, F. *Microfluid. Nanofluid.* **2015**, *19*, 1071−1090.
(16) Lim, S. W.; Abate, A. R. *Lab Chip* **2013**, *13*, 4563−4572.
(17) Ma, F.; Xie, Y.; Huang, C.; Feng, Y.; Yang, G. *PLoS One* **2014**, *9*, No. e116339.
(18) Zinchenko, A.; Devenish, S. R. A.; Kintses, B.; Colin, P. Y.; Fischlechner, M.; Hollfelder, F. *Anal. Chem.* **2014**, *86*, 2526−2533.
(19) Zilionis, R.; Nainys, J.; Veres, A.; Savova, V.; Zemmour, D.; Klein, A. M.; Mazutis, L. *Nat. Protoc.* **2017**, *12*, 44−73.
(20) Matuła, K.; Rivello, F.; Huck, W. T. *Adv. Biosyst.* **2020**, *4*, No. 1900188.
(21) Clark, I. C.; Delley, C. L.; Sun, C.; Thakur, R.; Stott, S. L.; Thaploo, S.; Li, Z.; Quintana, F. J.; Abate, A. R. *Anal. Chem.* **2020**, *92*, 14616−14623.
(22) Ma, S.; Huck, W. T.; Balabani, S. *Lab Chip* **2015**, *15*, 4291−4301.
(23) Sukovich, D. J.; Lance, S. T.; Abate, A. R. *Sci. Rep.* **2017**, *7*, No. 39385.
(24) Spiess, A. N.; Feig, C.; Ritz, C. *BMC Bioinf.* **2008**, *9*, No. 221.
(25) Quan, P. L.; Sauzade, M.; Brouzes, E. *Sensors* **2018**, *18*, No. 1271.
(26) Gong, Y.; Ogunniyi, A. O.; Love, J. C. *Lab Chip* **2010**, *10*, 2334−2337.
(27) White, A. K.; Heyries, K. A.; Doolin, C.; Vaninsberghe, M.; Hansen, C. L. *Anal. Chem.* **2013**, *85*, 7182−7190.
(28) Rajan, S.; Kierny, M. R.; Mercer, A.; Wu, J.; Tovchigrechko, A.; Wu, H.; Dall'Acqua, W. F.; Xiao, X.; Chowdhury, P. S. *Commun. Biol.* **2018**, *1*, No. 5.
(29) Eastburn, D. J.; Sciambi, A.; Abate, A. R. *PLoS One* **2013**, *8*, No. e62961.
(30) Beer, N. R.; Wheeler, E. K.; Lee-Houghton, L.; Watkins, N.; Nasarabadi, S.; Hebert, N.; Leung, P.; Arnold, D. W.; Bailey, C. G.; Colston, B. W. *Anal. Chem.* **2008**, *80*, 1854−1858.
(31) Zhang, Y.; Ho, Y.-P.; Chiu, Y.-L.; Chan, H. F.; Chlebina, B.; Schuhmann, T.; You, L.; Leong, K. W. *Biomaterials* **2013**, *34*, 4564−4572.
(32) Wacker, M. J.; Godard, M. P. *J. Biomol. Tech.* **2005**, *16*, 266−271.
(33) Islam, M. S.; Aryasomayajula, A.; Selvaganapathy, P. R. *Micromachines* **2017**, *8*, No. 83.

(34) Leuenberger, P.; Ganscha, S.; Kahraman, A.; Cappelletti, V.; Boersema, P. J.; Von Mering, C.; Claassen, M.; Picotti, P. *Science* **2017**, *355*, No. eaai7825.
(35) Marshall, J. L.; Doughty, B. R.; Subramanian, V.; Guckelberger, P.; Wang, Q.; Chen, L. M.; Rodriques, S. G.; Zhang, K.; Fulco, C. P.; Nasser, J.; Grinkevich, E. J.; Noel, T.; Mangiameli, S.; Bergman, D. T.; Greka, A.; Lander, E. S.; Chen, F.; Engreitz, J. M. *Proc. Natl. Acad. Sci. U.S.A.* **2020**, *117*, 33404−33413.
(36) Zanini, F.; Robinson, M. L.; Croote, D.; Sahoo, M. S.; Sanz, A. M.; Ortiz-Lasso, E.; Albornoz, L. L.; Rosso, F.; Montoya, J. G.; Goo, L.; Pinsky, B. A.; Quake, S. R.; Einav, S. *Proc. Natl. Acad. Sci. U.S.A.* **2018**, *115*, E12363−E12369.
(37) Saikia, M.; Burnham, P.; Keshavjee, S. H.; Wang, M. F. Z.; Heyang, M.; Moral-Lopez, P.; Hinchman, M. M.; Danko, C. G.; Parker, JSL.; De Vlaminck, I. *Nat. Methods* **2019**, *16*, 59−62.
(38) de Rutte, J.; Dimatteo, R.; Archang, M. M.; van Zee, M.; Koo, D.; Lee, S.; Sharrow, A. C.; Krohl, P. J.; Mellody, M.; Zhu, S.; Eichenbaum, J. V.; Kizerwetter, M.; Udani, S.; Ha, K.; Willson, R. C.; Bertozzi, A. L.; Spangler, J. B.; Damoiseaux, R.; Di Carlo, D. *ACS Nano* **2022**, *16*, 7242−7257.

## Recommended by ACS

**Large-Area Electronics-Enabled High-Resolution Digital Microfluidics for Parallel Single-Cell Manipulation**
Siyi Hu, Hanbin Ma, *et al.*
APRIL 18, 2023
ANALYTICAL CHEMISTRY
READ

**Parallel Dielectrophoretic Capture, Isolation, and Electrical Lysis of Individual Breast Cancer Cells to Assess Variability in Enzymatic Activity**
Joseph T. Banovetz, Robbyn K. Anand, *et al.*
MAY 12, 2023
ANALYTICAL CHEMISTRY
READ

**On-Chip Analysis of Protein Secretion from Single Cells Using Microbead Biosensors**
Diana F. Cedillo-Alcantar, Jose L. Garcia-Cordero, *et al.*
JANUARY 29, 2023
ACS SENSORS
READ

**Auto Flow-Focusing Droplet Reinjection Chip-Based Integrated Portable Droplet System (iPODs)**
Fengyi Liu, Bo Ma, *et al.*
APRIL 13, 2023
ANALYTICAL CHEMISTRY
READ

**Get More Suggestions >**


https://doi.org/10.1021/acs.analchem.2c03475
*Anal. Chem.* 2023, 95, 935−945